Combined Intensity- and Point-Based Cardiac Registration in the Presence of Landmark Errors

Mia Mojica* and Mehran Ebrahimi

Faculty of Science, University of Ontario Institute of Technology
mia.mojica@uoit.ca , mehran.ebrahimi@uoit.ca
http://www.ImagingLab.ca/

Abstract. Thin plate spline registration provides an effective and computationally efficient way of registering cardiac images, provided that the correct landmark locations and correspondences between the template and reference are defined. However, this technique fails to properly match images and introduces unnatural deformities to the transformed template in the presence of landmark errors. In this paper, we propose a novel registration model combining intensity and landmark information to register 2D cardiac images. The model can be adjusted to relax the landmark matching constraint and cater to landmark localization errors. The inclusion of an intensity-based similarity measure further improves image overlap by as much as 17%, along with a 31.05mm reduction in maximum landmark distance.

Keywords: Cardiac registration, Intensity and landmark registration, Thin plate spline

1 Introduction

Cardiac registration can generally be classified under two main categories: point-based and intensity-based registration. The former is driven by matching landmarks (LMs) that demarcate the positions of important anatomical structures. On the other hand, intensity-based registration deforms images by minimizing a distance measure that quantifies voxel similarity, such as the sum of squared distances (SSD) and the normalized gradient field (NGF) of two images [5].

Point-based registration can be viewed simply as an interpolation problem, with the optimal transformation being the function passing through each control point while satisfying other constraints, such as minimizing the oscillation of the interpolant. It is important to note, however, that point-based registration completely ignores the intensity of the images being registered. As a result, the image overlap away from the landmarks tends to suffer.

Point-based cardiac registration can be challenging and prone to errors since the selection of landmarks highly depends on the ability of the physician to mentally integrate information from different images [8]. In addition, the heart

* Corresponding author

only has few spatially accurate and repeatable anatomical landmarks. For instance, in [12], only the two papillary muscles and the inferior junction of the right ventricle were used to rigidly transform cardiac PET and US images. To circumvent the aforementioned issues, point-based registration is typically used either only as a preliminary step to correct cardiac scaling and orientation, or in conjunction with an approach that employs image intensity information in order to improve image overlap, as in [11]. In their paper, affine matching based on the left ventricular apex and the two right ventriculoseptal junctions in the valve plane orthogonal to the long axis of the heart was used to guide a subsequent hybrid landmark and intensity-based registration.

Here, we present the mathematical formulation of a model for intra-modality registration that simultaneously uses landmark and intensity information. This eliminates the need for a pre-registration step and makes the registration fully automatic. The model also allows for landmark matching constraint relaxation, which is useful in the presence of uncertainties in landmark correspondences. We validate the method on short axis slices of porcine hearts with automatically detected landmarks.

2 Thin Plate Spline Interpolation and Approximation

Thin plate splines (TPS) are a spline-based class of interpolating functions widely used in medical imaging. Introduced by Duchon in [3], TPS interpolates over scattered data while minimizing the bending energy of a thin metal plate on point constraints [2]. The idea of TPS was later used in point-based registration.

2.1 Thin Plate Spline Interpolation

Suppose that we want to find a smooth function $\theta : \Omega \subset \mathbb{R}^d \to \mathbb{R}^d$ for which

$$\theta(t_j) = r_j, \quad j = 1, \ldots, n.$$

Any interpolant satisfying the set of conditions above is automatically a minimizer of the functional

$$\mathcal{D}^{\mathrm{LM}}[\theta] = \sum_{j=1}^{n} \|\theta(t_j) - r_j\|^2 = 0.$$

Since this problem has many solutions, it is necessary to impose additional conditions to restrict our solution space. A meaningful option would be to find the interpolating function that minimizes the bending energy. With that, the original interpolation problem can be reformulated into the following:

$$\min_{\theta} \mathcal{S}^{\mathrm{TPS}}[\theta] := \min_{\theta} \int_{\Omega} \left\langle \nabla^2\theta(x), \nabla^2\theta(x) \right\rangle dx \quad \text{subject to } \mathcal{D}^{\mathrm{LM}}[\theta] = 0. \tag{1}$$

$\mathcal{S}^{\mathrm{TPS}}$ in Eq.(1) approximates the bending energy by an integration over the inner product of the Hessian of a function θ with itself. It has been shown that the unique solution [13] of the above optimization problem can be represented by a linear combination of radial basis functions ρ and a polynomial correction term [9]. That is,

$$\theta^i(x) = \sum_{j=1}^{n} c_j^i \rho\left(\|x - t_j\|\right) + w_0^i + w_1^i x^1 + \ldots + w_d^i x^d, \ i = 1, \ldots, d \tag{2}$$

In particular, for $d = 2$, ρ is given by $\rho(t) = t^2 \log t$.

In the presence of localization errors, it is possible to relax the interpolation condition in (1) by replacing the interpolation by approximation, so the optimization problem now reads

$$\min_{\theta} \mathcal{D}^{\mathrm{LM}}[\theta] + \beta \mathcal{S}^{\mathrm{TPS}}[\theta]. \tag{3}$$

The parameter $\beta \geq 0$ controls the smoothness of the minimizer and the mismatch of the data points. Note that $\beta = 0$ yields the interpolation problem in (1).

In the context of image registration, we can think of the point sets $\{r_j\}_{j=1}^n$ and $\{t_j\}_{j=1}^n$ as the sets of landmarks on the reference and template images, respectively. TPS interpolation provides a computationally efficient way of registering two images, provided that a one-to-one and accurately defined landmark correspondence is identified. Meanwhile, TPS approximation offers more flexibility for point sets with possible localization errors. Solving (1) and (3) via a system of linear equations is straightforward due to the linearity of their constraints in terms of the parameters of the optimal transformation.

3 Methods

Several approaches combining landmark- and intensity-based registration have already been proposed. Eriksson and Astrom introduced in [4] an intensity-based approach that focused on minimizing the SSD while restricting the solution space to thin plate spline mappings. In [7], another combined approach was presented. Similar restrictions were imposed on the solution space, with the NGF quantifying the image similarity instead. In addition, they regularized the model using the elastic regularizer.

We propose a registration model that uses both landmark and intensity information. Our aim is to maximize the overlap of images and of the correct LM pairs in the presence of localization and correspondence errors.

3.1 Mathematical model

Given a template image $\mathcal{T}$, we want to find a transformation $\theta^* : \Omega \subset \mathbb{R}^2 \to \mathbb{R}$ that minimizes the functional

$$\theta^* = \min_{\theta} \mathcal{D}^{\mathrm{LM}}[\theta] + \alpha \mathcal{D}^{\mathrm{INT}}[\theta] + \beta \mathcal{S}^{\mathrm{TPS}}[\theta] \tag{4}$$

$$\text{such that } \theta \text{ is a thin plate spline (2).}$$

As mentioned in the previous section, the term $\mathcal{S}^{\mathrm{TPS}}$ acts as a regularizer that relaxes the landmark matching constraint, thereby controlling the smoothness of the resulting deformation.

Meanwhile, the term $\mathcal{D}^{\mathrm{INT}}$ denotes the sum of squared intensity differences between a transformed version of the template and the reference. Its discrete analogue is given by

$$\mathcal{D}^{\mathrm{INT}}[\theta] = \sum_{x \in \Omega} \frac{h}{2} \Big(T\left[\theta(x)\right] - R(x) \Big)^2, \tag{5}$$

where h refers to the width of the grid constructed from the template and reference image domain. The ability to boost the image similarity between the transformed template and the reference while satisfying landmark matching or approximation conditions motivated the inclusion of the SSD similarity measure.

4 Experiments

We test the performance of our model on high resolution *ex-vivo* short axis images of porcine hearts at sub-millimetric spatial resolution (0.5×0.5 mm) in order to create an idealized case where neither cardiac nor respiratory motion does not affect the registration result. Data acquisition parameters are provided in [1]. As shown in Figure 1(a), points along the free wall of the right ventricle, the interventricular septum, and the left ventricular myocardium were chosen similar to [10]. To generate the template image and to find its landmarks, a known amount of deformation was applied to the reference slice and the reference landmarks.

The performance of the model for different values of α and β was investigated under the following three scenarios:

Case A. Correct landmark correspondence without any localization error
Case B. Correct landmark correspondence with a small localization error (29.32mm) in one of the template landmarks
Case C. Correct landmark correspondence in 10 out of the 11 landmark pairs and a small localization error in one of the template landmarks.

In all of the experiments, we computed the derivative of each component of the functional in (4) with respect to the parameters of the thin plate spline mapping and solved the minimization problem via gradient descent.

To determine the value of including the intensity term $\alpha\mathcal{D}^{\mathrm{INT}}$ and the smoothing term $\beta\mathcal{S}^{\mathrm{TPS}}$ in the model, we observed the effect of varying the magnitude of each term by considering different values of α and β, respectively, in every case that we considered.

Then, to quantify the match between the landmarks, we tracked the location of the correct template landmarks t_j^c after registration and computed the maximum component of the distance vector

$$\left\| \overrightarrow{D} \right\|_{\infty} = \max \left\{ \left\| t_j^c - r_j \right\| : j = 1, 2, \ldots, n \right\}.$$

This is especially useful for the last two cases, where landmarks were exposed to errors. In a way, this gauges how badly the registration is affected by such errors and how well the inclusion of the intensity and smoothing terms help to correct the overlap in spite of the errors.

We also calculated the Jaccard similarity to measure the image overlap before and after registration. Given a template $\mathcal{T}$ and a reference $\mathcal{R}$, the Jaccard similarity coefficient pre- and post-registration are defined as

$$J\left[\mathcal{T},\mathcal{R}\right]=\frac{\left|\mathcal{T}\cap\mathcal{R}\right|}{\left|\mathcal{T}\cup\mathcal{R}\right|}\quad\text{and}\quad J\left[\mathcal{T}\left[\theta\right],\mathcal{R}\right]=\frac{\left|\mathcal{T}\left[\theta\right]\cap\mathcal{R}\right|}{\left|\mathcal{T}\left[\theta\right]\cup\mathcal{R}\right|},$$

respectively.

5 Results and Discussion

Shown in Figure 1(a) and (b) are the reference and template images used in the experiments and the correct location of the landmarks. The pre-registration Jaccard coefficient of the two images is 53.84%, while the initial maximum entry of the distance vector from the reference to the template landmarks is 24.14mm. Since TPS registration ($\alpha=\beta=0$) is widely used in medical image registration, we will be using the results obtained from blindly applying the technique as a baseline for every set of experiment described in the previous section. We will then investigate how the model affects the deformation of images visually and quantify its performance based on the overall landmark separation and image similarity after registration.

As expected, TPS performed well when the correct pairing and locations of the landmarks were used to guide the registration (see Figure 2(a)). Image overlap increased by almost forty percent, to 91.24%, and the maximum landmark distance went down to 8.20×10^{-13} mm. Our model yielded similar results for this scenario. We can see from the first column in Figure 3 that increasing the magnitude α of the intensity term resulted in comparable overlaps between the registered template and the reference image. Naturally, relaxing the matching constraint by increasing the value of β gave poor results when there is an accurate correspondence between landmarks to begin with.

Shown in Figures 2(b) and (c) and the last two columns in Figure 3 are the results when TPS registration was applied blindly to landmarks with errors. It can be seen that unnatural deformities were introduced to the registered image by the wrong placement of landmarks. Aside from the obvious jump in maximum

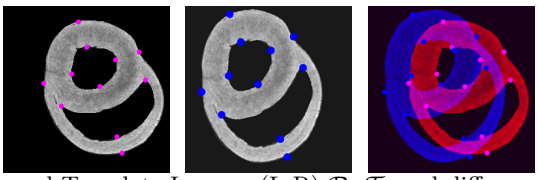

Fig. 1: Reference and Template Images. (L-R) $\mathcal{R}$, $\mathcal{T}$, and difference image $|\mathcal{T}-\mathcal{R}|$.

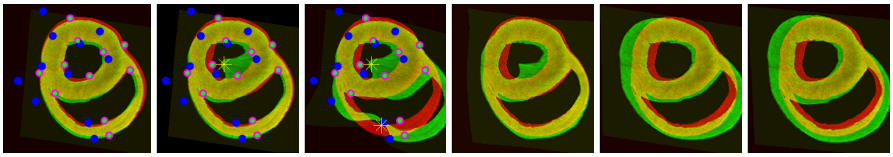

(a) TPS-0Er. **(b)** TPS-1Er. **(c)** TPS-2Er. **(d)** $\beta = 0$ **(e)** $\beta = 1$ **(f)** $\beta = 10$

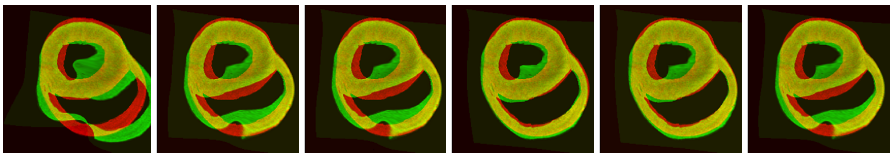

(g) $\alpha = 0$ **(h)** $\alpha = 10^{-5}$ **(i)** $\alpha = 10^{-4}$ **(j)** $\alpha = 10^{-3}$ **(k)** $\alpha = 10^{-2}$ **(l)** $\alpha = 10^{-1}$

Fig. 2: Registration Results. (a)-(c) Baseline/TPS results ($\alpha = \beta = 0$), (c)-(d) demonstrates the effect of increasing the magnitude β of the smoothing term (with $\alpha = 0.01$) on deformities caused by a localization error, (g)-(l) shows the benefit of adding the intensity term to the model. Note that these are fused images of the registered template and the reference. Red=regions exclusively in $\mathcal{R}$, green=exclusively in the registered template $\mathcal{T}[\theta]$, yellow=regions where the two overlapped

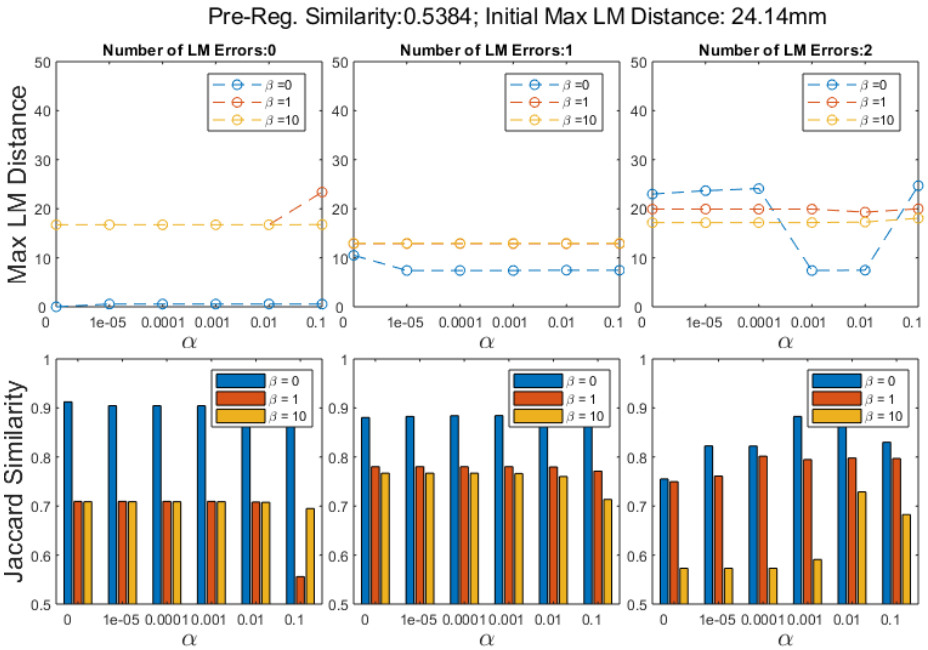

Fig. 3: Summary of Results. Results of using reference and template LMs that exhibit (Column 1) no localization error, (Column 2) a small localization error (29.32mm) in one of the template LMs, (Column 3) correct correspondence in 10 out of the 11 LM pairs and a small localization error in one of the template LMs. First row gives the max. of the vector of distances (in mm) between reference and correct template LM pairs. Second row shows the Jaccard coefficients for different values of the model parameters.

landmark distance, the post-registration image overlap dropped by 3% and 16% for Case A and Case B, respectively.

For Case B, we see from Figure 3 that the final Jaccard similarities when $\beta = 0$ are at par with the baseline result. Improvements resulting from our method are more evident if we look at the maximum landmark distance after adding the intensity term (i.e., by setting $\alpha > 0$). It decreased from 10.50mm to 7.40mm when $\alpha = 0$. More importantly, if we look at Figures 2(d)-(f) and compared it against the benchmark in Figure 2(b), we can see that the deformity introduced by the landmark error became less pronounced with the inclusion of the intensity term in the model. The deformity even disappeared when the smoothing term was added (i.e., when $\beta > 0$), although with some image similarity tradeoffs.

Finally, for Case C, where we have 2 errors – 1 small localization error and 1 incorrect template-reference landmark correspondence – observe from the third column in Figure 3 that our model outperformed the baseline for every value of α used and for $\beta = 0.1$. The best overlap and least maximum LM distance occurred when $\alpha = 0.01$ and $\beta = 0$. This tells us that our model can compensate for LM correspondence and localization errors. If we look at the results in Figures 2(g)-(l) and compare them against the TPS registration result in Figure 2(c), we can conclude that adding the intensity term indeed helped to reduce the deformities caused by these errors.

To summarize, we found that our method consistently performed at par with the TPS approach whenever landmarks are correctly identified or only small errors are present in the data. In cases where there are significant LM errors, our method yielded better overlaps and matching of the correct LM pairs.

6 Conclusions

Thin plate spline-based registration provides an effective and computationally efficient way of registering cardiac images, provided that correct landmark locations and correspondences between the template and reference are defined. However, identifying cardiac landmarks is prone to error because there are only few accurate anatomical landmarks and because its position changes along with cardiac contraction and thorax motion due to respiration. In the presence of landmark errors, TPS registration fails to properly register cardiac images and could introduce unnatural deformities to the transformed cardiac template.

Here, we proposed a novel registration model combining intensity and landmark information to match pairs of 2D cardiac images. The model can be adjusted to relax the landmark matching constraint to cater to landmark localization errors. Most importantly, the inclusion of the intensity term helped to improve the overlap between the transformed template and reference image while still satisfying the specified landmark matching or approximation conditions. Our experiments demonstrated that this new method consistently yields good registration overlaps and outperforms the widely used TPS registration in cases where there are significant LM errors.

References

1. Bookstein, F.L.: Principal warps: Thin-plate splines and the decomposition of deformations. IEEE Transactions on pattern analysis and machine intelligence 11(6), 567–585 (1989)
2. Duchon, J.: Splines minimizing rotation-invariant semi-norms in sobolev spaces. In: Constructive theory of functions of several variables, pp. 85–100. Springer (1977)
3. Eriksson, A.P., Astrom, K.: Bijective image registration using thin-plate splines. In: 18th International Conference on Pattern Recognition (ICPR'06). vol. 3, pp. 798–801. IEEE (2006)
4. Fischer, B., Modersitzki, J.: Combining landmark and intensity driven registrations. In: PAMM: Proceedings in Applied Mathematics and Mechanics. vol. 3, pp. 32–35. Wiley Online Library (2003)
5. Helm, P.A.: A novel technique for quantifying variability of cardiac anatomy: Application to the dyssynchronous failing heart. (2004)
6. Lam, K.C., Lui, L.M.: Landmark-and intensity-based registration with large deformations via quasi-conformal maps. SIAM Journal on Imaging Sciences 7(4), 2364–2392 (2014)
7. Lange, T., Papenberg, N., Heldmann, S., Modersitzki, J., Fischer, B., Lamecker, H., Schlag, P.M.: 3d ultrasound-ct registration of the liver using combined landmark-intensity information. International journal of computer assisted radiology and surgery 4(1), 79–88 (2009)
8. Makela, T., Clarysse, P., Sipila, O., Pauna, N., Pham, Q.C., Katila, T., Magnin, I.E.: A review of cardiac image registration methods. IEEE Transactions on medical imaging 21(9), 1011–1021 (2002)
9. Modersitzki, J.: FAIR: Flexible algorithms for image registration, vol. 6. SIAM (2009)
10. Nielsen, P., Le Grice, I., Smaill, B., Hunter, P.: Mathematical model of geometry and fibrous structure of the heart. American Journal of Physiology-Heart and Circulatory Physiology 260(4), H1365–H1378 (1991)
11. Peyrat, J.M., Sermesant, M., Pennec, X., Delingette, H., Xu, C., McVeigh, E.R., Ayache, N.: A computational framework for the statistical analysis of cardiac diffusion tensors: application to a small database of canine hearts. IEEE Transactions on medical imaging 26(11), 1500–1514 (2007)
12. Pop, M., Ghugre, N.R., Ramanan, V., Morikawa, L., Stanisz, G., Dick, A.J., Wright, G.A.: Quantification of fibrosis in infarcted swine hearts by ex vivo late gadolinium-enhancement and diffusion-weighted MRI methods. Physics in medicine and biology 58(15), 5009 (2013)
13. Savi, A., Gilardi, M.C., Rizzo, G., Pepi, M., Landoni, C., Rossetti, C., Lucignani, G., Bartorelli, A., Fazio, F.: Spatial registration of echocardiographic and positron emission tomographic heart studies. European journal of nuclear medicine 22(3), 243–247 (1995)
14. Wahba, G.: Spline models for observational data, vol. 59. Siam (1990)